Supplementary Material
GESTATIONAL-AGE-DEPENDENT DEVELOPMENT OF THE NEONATAL METABOLOME

Madeleine Ernst (1,2), Simon Rogers (3), Ulrik Lausten-Thomsen, MD (4), Anders Björkbom (1,2), Susan Svane Laursen (1,2), Julie Courraud (1,2), Anders Børglum (2,5,6,7), Merete Nordentoft (2,8,9), Thomas Werge (2,9,10,11), Preben Bo Mortensen (2,12,13), David M Hougaard (1,2) Arieh S.Cohen (1,2)

(1) Section for Clinical Mass Spectrometry, Department of Congenital Disorders, Danish Center for Neonatal Screening, Statens Serum Institut, Copenhagen, Denmark
(2) iPSYCH, The Lundbeck Foundation Initiative for Integrative Psychiatric Research, Copenhagen, Denmark
(3) School of Computing Science, University of Glasgow, Glasgow G12 8QQ, United Kingdom
(4) Department of Neonatology, Copenhagen University Hospital Rigshospitalet, Copenhagen, Denmark
(5) Center for Genomics and Personalized Medicine, Aarhus, Denmark
(6) Department of Biomedicine – Human Genetics, Aarhus University, Aarhus, Denmark
(7) Bioinformatics Research Centre, Aarhus University, Aarhus, Denmark
(8) Danish Research Institute for Suicide Prevention, Copenhagen Research Center for Mental Health (CORE), Mental Health Center Copenhagen, Copenhagen, Denmark
(9) Department of Clinical Medicine, Faculty of Health and Medical Sciences, University of Copenhagen, Copenhagen, Denmark
(10) Center for GeoGenetics, Globe Institute, Faculty of Health and Medical Sciences, University of Copenhagen, Copenhagen, Denmark
(11) Institute of Biological Psychiatry, Mental Health Centre Sct. Hans, Mental Health Services Capital Region of Denmark, Copenhagen, Denmark
(12) NCRR - National Centre for Register-based Research, Aarhus University, Aarhus, Denmark
(13) CIRRAU - Centre for Integrated Register-based Research at Aarhus University, Aarhus, Denmark

Supplementary Methods

Metabolomic Profiling

LC-MS/MS allows for the simultaneous detection of thousands of peaks, corresponding to individual ions with a unique mass to charge (*m/z*) ratio, retention time and fragmentation pattern, which can be used for chemical structural annotation [da Silva et al., 2018]. All solvents were of LCMS-grade and were purchased from Thermo Fisher Scientific (Waltham, MA, USA). 45 µL of the residual extracts of dried blood spots used for routine neonatal screening prepared through the NeoBase™ Non-derivatized MSMS kit (PerkinElmer, MA, USA) were dried down under a gentle flow of nitrogen at room temperature in a 96-well plate. Prior to analysis the extracts were reconstituted in 45 µL of water. The LC-MS/MS platform consisted of a Thermo Scientific Q-Exactive Orbitrap mass spectrometer coupled to a Dionex Ultimate 3000 UPLC with a binary pump, column oven and Thermo CTC sampler (Thermo Fisher Scientific). Chromatographic separation was performed with an Acquity UPLC BEH C18 column (130 Å, 2.1 mm x 100 mm, 1.7 µm) preceded by a Acquity UPLC BEH C18 VanGuard pre-column (130 Å, 2.1 mm x 5 mm, 1.7 µm) (Waters Corporation, Waltham, MA, USA).

The mobile phase consisted of solvent A (99.9% water and 0.1% formic acid) and B (99.9% methanol and 0.1% formic acid). The gradient of the mobile phase was as follows: 0-1 min, 100% solvent A at 0.3 ml/min; 1-9 min, from 100% solvent A to 100% solvent B (gradient ramp) at 0.3 ml/min. In between each sample the chromatographic column was washed using the following gradient: 10-10.3 min, from 0.3 ml/min to 0.5 ml/min 100% solvent B; 10.3-12 min, 100% B at 0.5 ml/min; 12-12.5 min, from 0.5 ml/min to 0.3 ml/min 100% solvent B; 12.5-13 min, from 100% solvent B to 100% solvent C (24.95% water, 24.95% methanol, 24.95% acetonitrile, 24.95% isopropanol, and 0.2% formic acid); 13-14 min, 100% solvent C; 14-14.5 min, from 100% solvent C to 100% solvent A; 14.5-20 min, 100% solvent A. Samples were maintained at + 4 °C in the autosampler, 15 µL were loaded to the column with a flow rate of 0.3 ml/min and a column temperature of 50 °C.

Tandem mass spectrometric analysis was performed in positive ionization mode, with spray voltages +3.8 and -2.5 kV, capillary temperature 350 °C, sheath gas flow rate 32, auxiliary gas flow rate 8, and S-lens RF level 50. For full MS (MS1), the parameters were set as follows: microscans: 1, resolution: 70'000, AGC target: 1E6, maximum IT: 250 ms, number of scan ranges: 1, scan range from 87 to 1100 *m/z* and spectrum data type: profile. For dd-MS^2 (MS/MS), the parameters were set as follows: microscans: 1, resolution: 17'500, AGC target: 1E5, maximum IT: 50 ms, loop count: 3, MSX count: 1, TopN: 3, isolation window: 1.5 *m/z*, isolation offset 0 *m/z*, scan range 200 to 2000 *m/z*, stepped NCE (17.5, 35, 52.5), spectrum data type: profile. For dd, the parameters were set as follows: minimum AGC target: 1E3, intensity threshold: 2E4, apex trigger: 2 to 4 s, charge exclusion: 2-8 and above 8, peptide match: off, exclude isotopes: on and dynamic exclusion: 25s. Diisooctyl phthalate (*m/z* 391.2843) was used as lock mass.

ThermoFisher .raw files were exported to the .mzML format using ProteoWizard's MSConvert (version 3.0) [Kessner et al., 2008] and preprocessed using MZmine (version 2.40.1) [Pluskal et al., 2010]. Data was cropped, with chromatogram retention time from 0.5 to 10 min retained. Mass lists were created with MS1 intensity above 1E4 and MS2 intensity above 0 retained. The chromatogram was built through the ADAP chromatogram builder [Myers et al., 2017] by using the following parameters: minimum group size of scans: 3, group intensity threshold:

1E4, minimum highest intensity: 3E4, and *m/z* tolerance: 0.01 *m/z* or 10 ppm. The chromatogram was further deconvoluted using the MEDIAN *m/z* center calculation, *m/z* range for MS2 scan pairing: 0.01 Da and retention time range for MS2 scan pairing: 0.2 min. The wavelets (ADAP) algorithm was used for deconvolution with parameters set to: S/N threshold: 20, S/N estimator: intensity window SN, minimum feature height: 30'000, coefficient/area threshold: 110, peak duration range: 0 to 2 and retention time wavelet range: 0 to 0.1. The peaks were deisotoped using the isotopic peak grouper function, with parameters set to: *m/z* tolerance: 0.01 *m/z* or 10 ppm, retention time tolerance: 0.1 min, maximum charge: 2, representative isotope: most intense. Peaks from all samples were aligned, by using the join aligner function with parameters set to, *m/z* tolerance: 0.01 *m/z* or 10 ppm, retention time tolerance: 0.5 min, weight for *m/z*: 75, weight for retention time: 25. Finally, two feature tables were exported in the .csv format. One feature table containing all extracted mass spectral features and another feature table filtered for mass spectral features with associated fragmentation spectra (MS2). Aggregated MS2 fragmentation spectra were exported in the .mgf format and submitted to feature-based mass spectral molecular networking through GNPS [Wang et al., 2016; Watrous et al., 2012; Nothias et al., 2019]. For statistical analysis, mass spectral features with a relative intensity less than 20 times the mean relative intensity of all blank samples were removed and feature intensities were normalized by the total ion current. Chemical structural relatedness of all mass spectral features was visualized within Cytoscape 3.7.2 [Shannon et al., 2003]. Raw and preprocessed mass spectrometry data, anonymized sample metadata as well as MZmine preprocessing parameter batch files are available upon request.

Statistical Analyses

To predict gestational age from the neonatal metabolome, we adapted the tenfold cross-validation (CV) implementation of the least absolute shrinkage and selection operator method (LASSO) from Wilmanski and collaborators (2019), using the Jupyter notebook publicly available at : https://github.com/PriceLab/ShannonMets/blob/master/FiguresNotebooks/LASSO_RIDGE_METABOLOMICS_ANALYSIS.ipynb. This also included comparison to a Ridge regression to assess the performance of both models in predicting gestational age. Analysis was performed as described in Wilmanski and co-workers (2019), with all metabolites being standardized to mean 0 and unit variance before analysis and both LASSO and Ridge regression fitted with an intercept. Each penalized regression model was trained on 90% of the cohort with tenfold CV and the metabolome-predicted gestational age was predicted for the 10% of samples not used for model optimization. Repeating this process ten times results in a test set of metabolome-predicted gestational ages and ten different β-coefficients for each metabolite. The R^2 was computed using the mean of all R^2 of the ten out-of-sample predictions and Pearsons' r was calculated through the observed gestational and metabolome-predicted gestational age of all samples.

Hypergeometric testing was used to identify chemically structurally related molecular families overrepresented with metabolites correlating with gestational age. To this end, results from the univariate correlation analysis (Kendall's Tau) were combined with the molecular network to extract molecular families significantly related with gestational age. Molecular families containing more metabolites significantly correlated (P value < 0.01 before FDR correction)

with gestational age than would be expected by chance were identified using a hypergeometric test parameterised by the total number of metabolites, the number of significantly correlated metabolites with gestational age and the size of the family of interest. A P value was obtained by computing the probability of observing the observed number of significant metabolites (or more) under the null assumption that families are formed by drawing metabolites uniformly without replacement.

Metabolite Identification

A mass spectral molecular network was created through the Global Natural Products Social Molecular Networking Platform (GNPS) [Wang et al., 2016] (http://gnps.ucsd.edu) using the feature-based molecular networking workflow [Nothias et al., 2019]. The data was filtered by removing all MS/MS fragment ions within +/- 17 Da of the precursor *m/z*. MS/MS spectra were window filtered by choosing only the top 6 fragment ions in the +/- 50Da window throughout the spectrum. The precursor ion mass tolerance was set to 0.02 Da and a MS/MS fragment ion tolerance of 0.02 Da. A network was then created where edges were filtered to have a cosine score above 0.7 and more than 4 matched peaks. Further, edges between two nodes were kept in the network if and only if each of the nodes appeared in each other's respective top 10 most similar nodes. Finally, the maximum size of a molecular family was set to 100, and the lowest scoring edges were removed from molecular families until the molecular family size was below this threshold. The spectra in the network were then searched against the GNPS spectral libraries. The library spectra were filtered in the same manner as the input data. All matches kept between network spectra and library spectra were required to have a cosine score above 0.7 and at least 4 matched peaks. In Supplementary figures, "NAP-Fusion" refers to annotations retrieved through the Network Annotation Propagation (NAP) workflow [da Silva et al., 2018], as part of MolNetEnhancer [Ernst et al., 2019].

Supplementary Results

LASSO regression

Ride regression has a tendency to perform better for datasets, where predictor variables are highly collinear and a large number of small effects is distributed across the predictor variables [Wilmanski et al., 2019; Tibshirani, 1996]. As for Wilmanski and collaborators (2019), the LASSO model outperformed Ridge regression for our dataset. An average of 21% of variance could be explained by gestational age using Ridge regression with tenfold CV, when compared to 37% using LASSO regression with tenfold CV. This indicates that blood metabolites predicting gestational age in the cohort are largely independent [Wilmanski et al., 2019]. Indeed, when assessing collinearity among the 93 metabolites selected by the LASSO model, only 52 out of the 8556 metabolite-metabolite comparisons were found to be highly collinear ($|r| > 0.80$).

Supplementary Discussion

We observed that structural analogues of mannitol and cellobiose are increased in preterm infants (Supplementary Data 3). Mannitol is a surprising finding as it is not absorbed through the gut and is thus not a common sugar molecule found in blood. Cellobiose is a degradation product of cellulose, which can not be metabolized by humans [Satouchi et al., 1998]. Thus we speculate that the mass spectral feature observed here is a close structural analogue of cellobiose, such as other glucose dimers that is a result of peritoneal nutrient solution which has previously been observed in the blood of preterm neonates [Chace et al., 2010]. Spectral mirror plots of both sugar molecules are available in Supplementary Data 2.

Carnitines and bile acids may be produced endogenously or absorbed through diet. Microbes are known to have a profound effect on carnitine as well as bile acid metabolism. When reaching the gut, microbes may chemically structurally modify products of bile and carnitine metabolism. Microbially modified carnitines and bile acids may re-enter blood circulation through the gut and in more recent years have shown to play an important role in gastrointestinal and metabolic diseases [Lloyd-Price et al., 2019; Meadows and Wargo, 2015; Singh et al., 2019]. Here, we found that most blood carnitine structural analogues were correlated positively with gestational age (17 out of 21, Supplementary Figure 6, Supplementary Data 3). This finding corroborates with previous targeted metabolite analyses in preterm newborns [Sanches-Pintos et al., 2016]. Neonates have reduced endogenous carnitine biosynthesis and rely on placental transfer, which occurs mainly during the third trimester [Sanches-Pintos et al., 2016; Meadows and Wargo, 2015]. Multiple studies have reported beneficial effects of carnitine on metabolic health via stimulation of glucose oxidation, including protection against insulin-resistance and myocardial ischemia injury [Ussher et al., 2013]. More recent studies have also highlighted microbiome-associated carnitine structural analogues with anti-inflammatory properties [Lloyd-Price et al., 2019; Morton et al., 2019]. Dietary L-carnitine on the other hand may serve as a source of gut microbiota-derived trimethylamine N-oxide (TMAO), which has been associated with increased cardiovascular risk [Meadows and Wargo, 2015; Wang et al., 2011]. Primary bile acids are metabolized to

unconjugated and secondary bile acids by microbes in the gut through deconjugation and dehydroxylation reactions, respectively [Singh et al., 2019]. Here we found that a majority of the chemically structurally annotated bile acids are primary and correlate negatively with gestational age. This finding is in agreement with previous studies reporting over 90% of all bile acids found in neonatal serum as primary [Zöhrer et al., 2016]. Few chemical structural analogues of secondary bile acids in the blood of neonates might be reflective of the immaturity of the colonic microbiome [Groer et al., 2014; Zöhrer et al., 2016]. Overall serum bile acid levels were previously found to be higher in preterm neonates born before 29 weeks of gestation [Zöhrer et al., 2016], which is in agreement with our finding that a majority of bile acids detected here correlate negatively with gestational age. Carnitines as well as bile acids form a wide variety of chemical structural analogues, challenging chemical structural annotation through MS/MS fragmentation patterns, with chemically structurally different molecules exhibiting close similarities in mass spectral fragmentation patterns. Thus chemical structural annotation could in most cases only be performed at the level of putatively characterized compound classes, corresponding to a level 3 metabolite annotation according to the Metabolomics Standard Initiative's reporting standards [Sumner et al., 2007]. Further studies would be needed to verify chemical structural annotation and results described here should be interpreted with care.

Gut microbiota have also been shown to play an important role in the catabolism of amino acids and phosphatidylcholine. For example, imidazole propionate, found to correlate negatively with gestational age, is a microbially-produced histidine catabolite [Koh et al., 2018]. Similarly, phenylacetylglutamine, a product of microbial metabolism of glutamine, was found to correlate negatively with gestational age [Bogiatzi et al., 2018]. Gut microbiota were recently shown to also play an important role in tryptophan metabolism [Dehhaghi et al., 2019; Roager et al., 2018]. Here we found that kynurenic acid, a catabolite of tryptophan metabolism correlates negatively with gestational age. Gut microbiota were also shown to be implicated in phosphatidylcholine catabolism. Here, we found that a phosphatidylcholine with *m/z* 440.2773 correlated negatively with gestational age, whereas betaine, a possible catabolite of dietary phosphatidylcholine correlated positively with gestational age. Gut microbiota were shown to be directly involved in phosphatidylcholine catabolism to TMAO, however our mass spectral method did not capture TMAO (*m/z* below 80) (Figure 2) [Wang et al., 2011].

Polyamines such as spermine and spermidine, here found to correlate negatively with gestational age, were shown to play an important role in fetal development and in regulating intestinal epithelial integrity by modulating the expression of various growth-related genes [Hussain et al., 2017; Timmons et al., 2012]. Besides being synthesized by the host or imported from the diet, polyamines may also be produced by intestinal microflora [Hussain et al., 2017].

Supplementary Table 1. Distribution of study cohort by sex, gestational age, age at sampling, multiplicity and mother's age. Prematurity categories were adapted from Wilson and collaborators (2016).

	N (%)
Sex	
Male	86 (58.1)
Female	62 (41.9)
Age at sampling	
2 days	69 (46.6)
3 days	79 (53.4)
Multiple births	
No	143 (96.6)
Yes	5 (3.4)
Age of mothers	
<20 years	0
20-24 years	14 (9.5)
25-29 years	47 (31.8)
30-34 years	52 (35.1)
35-39 years	28 (18.9)
≥ 40 years	7 (4.7)
Gestational age (prematurity category)	
	N (%) [mean birth weight; birth weight range]
28 weeks (very preterm)	10 (6.8) [1200; 850-1995]
29 weeks (very preterm)	10 (6.8) [2037.89; 840-3916]

30 weeks (very preterm)	8 (5.4) [1725.5; 1020.32]
31 weeks (very preterm)	10 (6.8) [1598.0; 920, 1961]
32 weeks (very preterm)	10 (6.8) [1974.22; 1310, 3196]
33 weeks (near term)	10 (6.8) [1935.70; 1109, 2592]
34 weeks (near term)	10 (6.8) [24332.20; 1615, 3685]
35 weeks (near term)	10 (6.8) [2550.10; 1580, 3240]
36 weeks (near term)	10 (6.8) [2850.2; 2590, 3190]
37 weeks (term)	10 (6.8) [2960.2; 1940, 3620]
38 weeks (term)	10 (6.8) [3417.70; 3078, 4345]
39 weeks (term)	10 (6.8) [3486.20; 2730, 4260]
40 weeks (term)	10 (6.8) [3932.50; 3180, 4820]
41 weeks (late term)	10 (6.8) [3883.50; 2940, 4360]
42 weeks (late term)	10 (6.8) [3913.80; 2986, 4760]

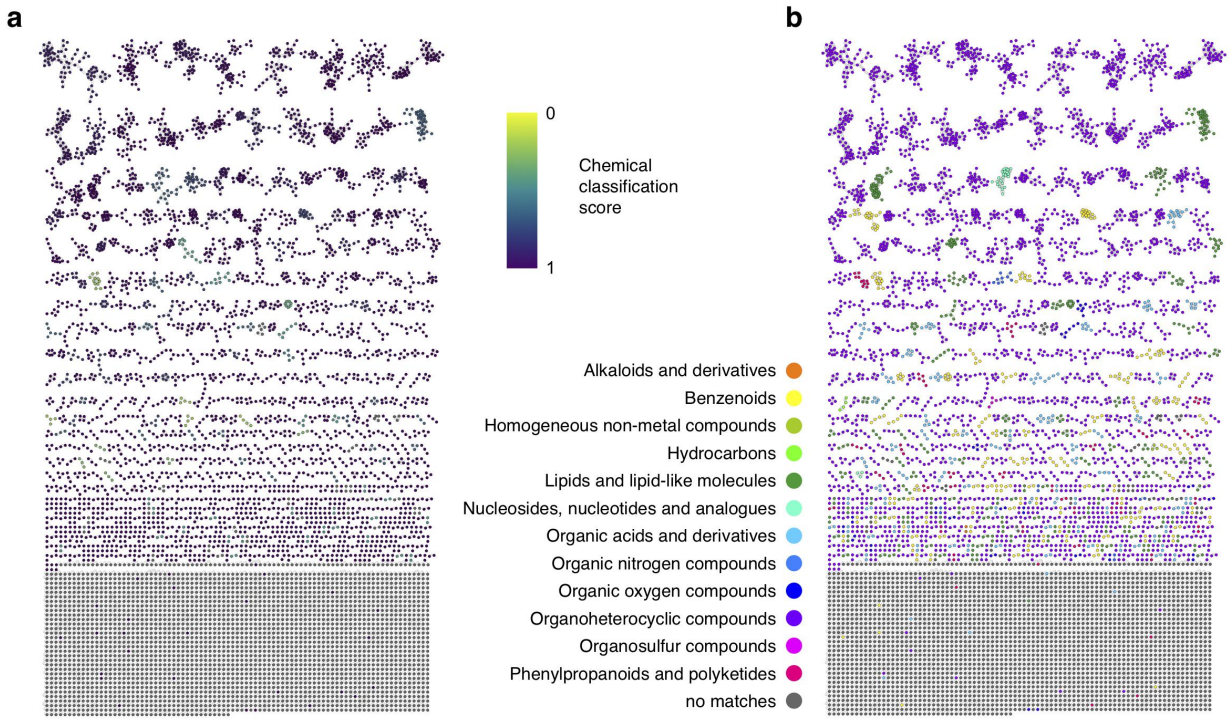

Supplementary Figure 1: Global mass spectral molecular network of neonatal dried blood spots with varying gestational ages. **a**. Molecular network colored by chemical classification scores. A chemical classification score of 1 means that all nodes within a given molecular family had at least one *in silico* chemical structural hit [Ernst et al., 2019] **b**. Molecular network colored by putative chemical superclasses retrieved through the MolNetEnhancer workflow and ClassyFire [Ernst et al., 2019; Djoumbou et al., 2016]. Each node in the network represents a mass spectral feature, which we here use as a proxy for a metabolite. Connected nodes represent high tandem mass spectral similarity, implying high chemical structural similarity.

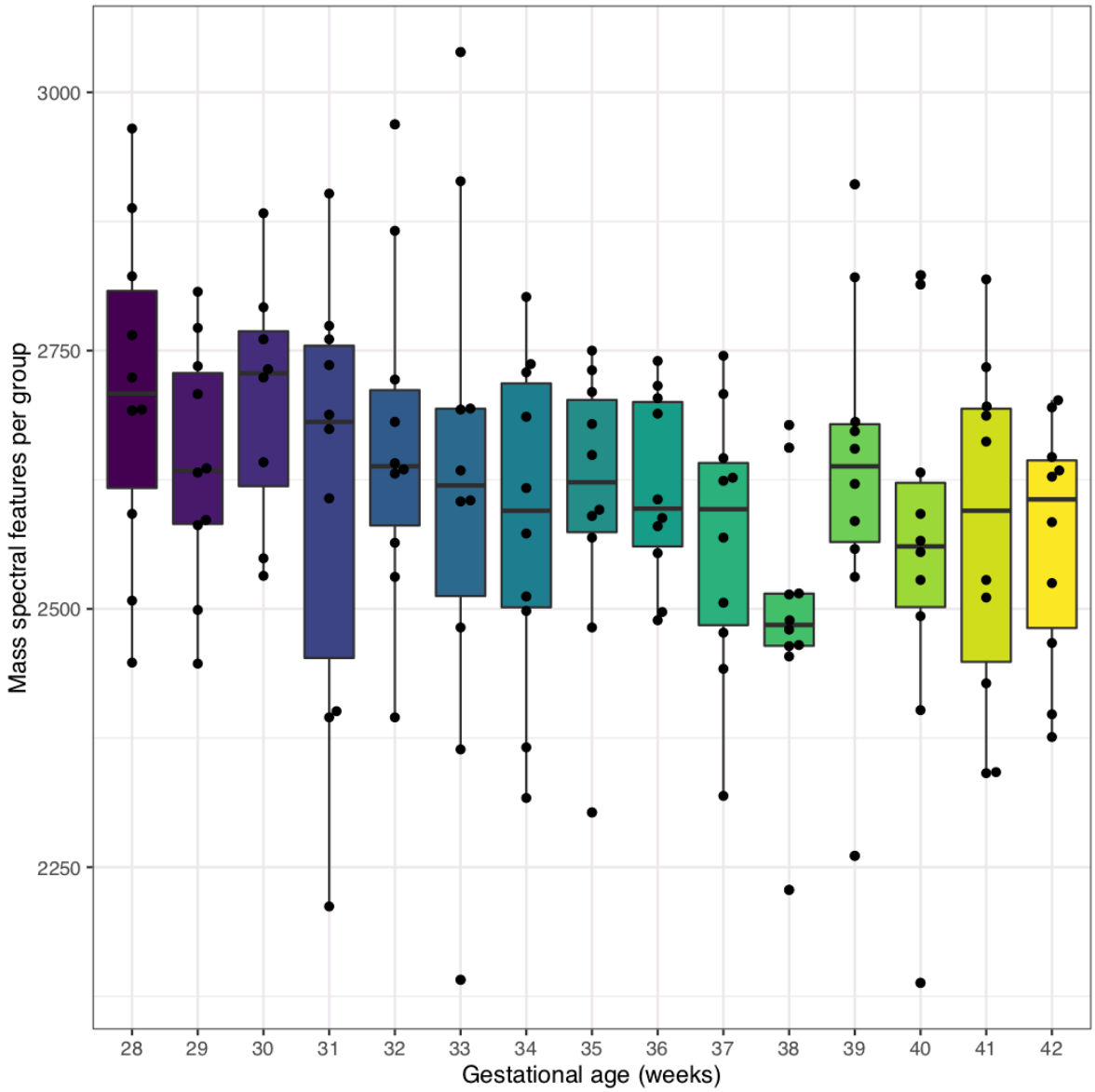

Supplementary Figure 2: Box plots for number of mass spectral features stratified across different gestational ages. The mean number of mass spectral features was found to correlate significantly with gestational age (Kendall's Tau = -0.2, $P < 0.05$).

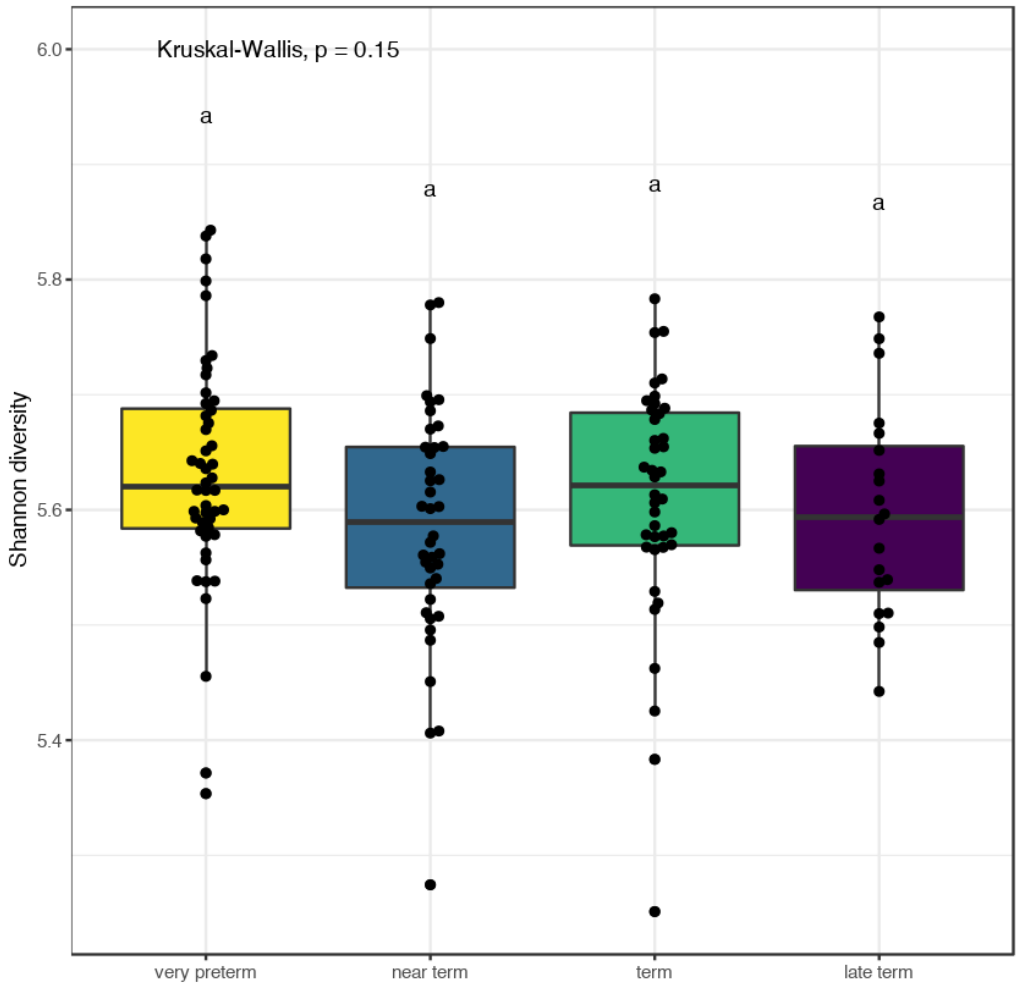

Supplementary Figure 3: Box plots for Shannon diversity stratified across different prematurity categories. No significant differences were found across mean Shannon diversities per prematurity category (Kruskal-Wallis, P = 0.15).

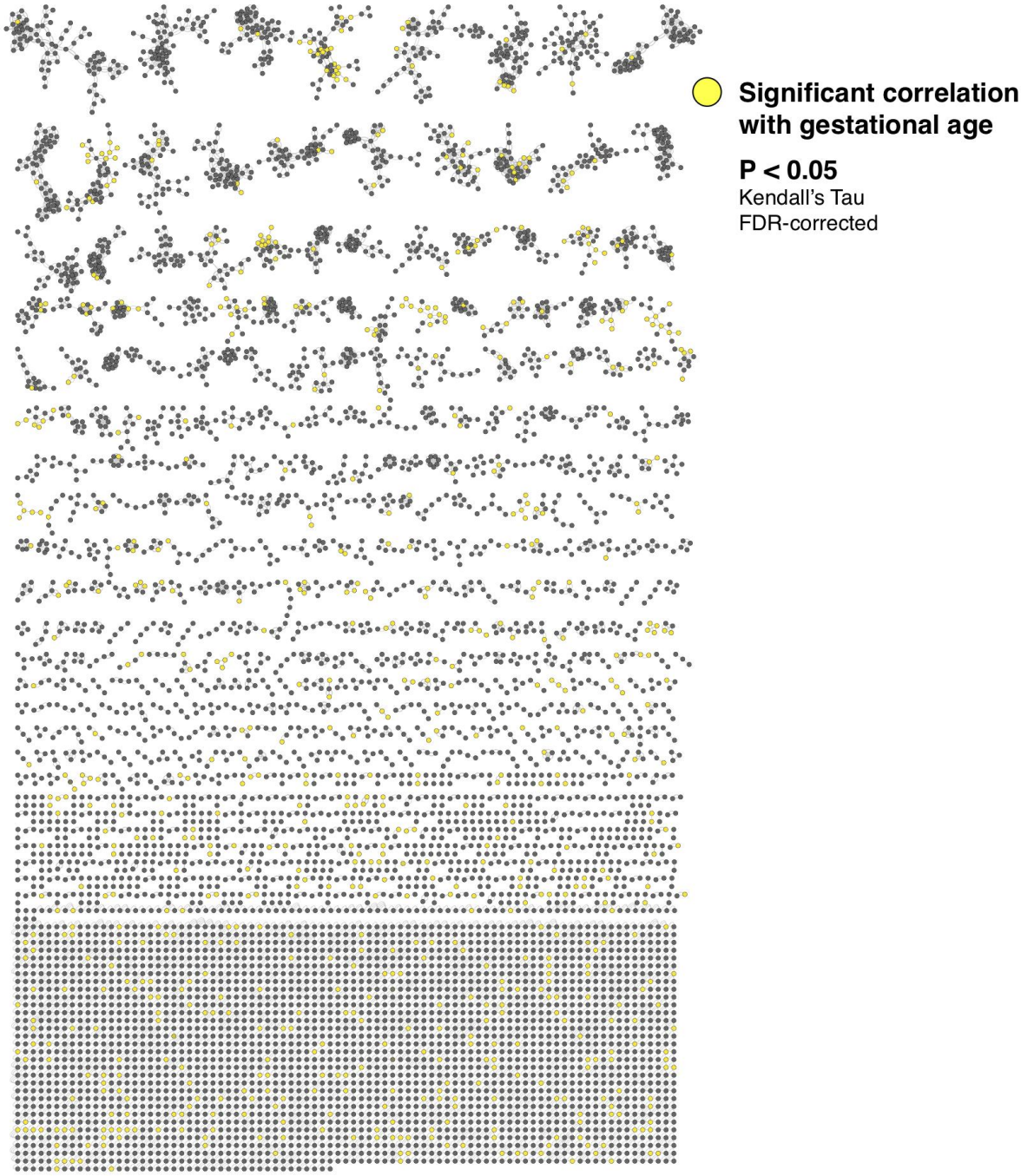

Supplementary Figure 4: Global mass spectral molecular network with metabolites significantly correlating with gestational age highlighted (Kendall's Tau, false-discovery-rate-adjusted P < 0.05). Out of 6053 mass spectral features, 744 were found to correlate significantly with gestational age. Each node in the network represents a mass spectral feature, which we here use as a proxy for a metabolite. Connected nodes represent high tandem mass spectral similarity, implying high chemical structural similarity.

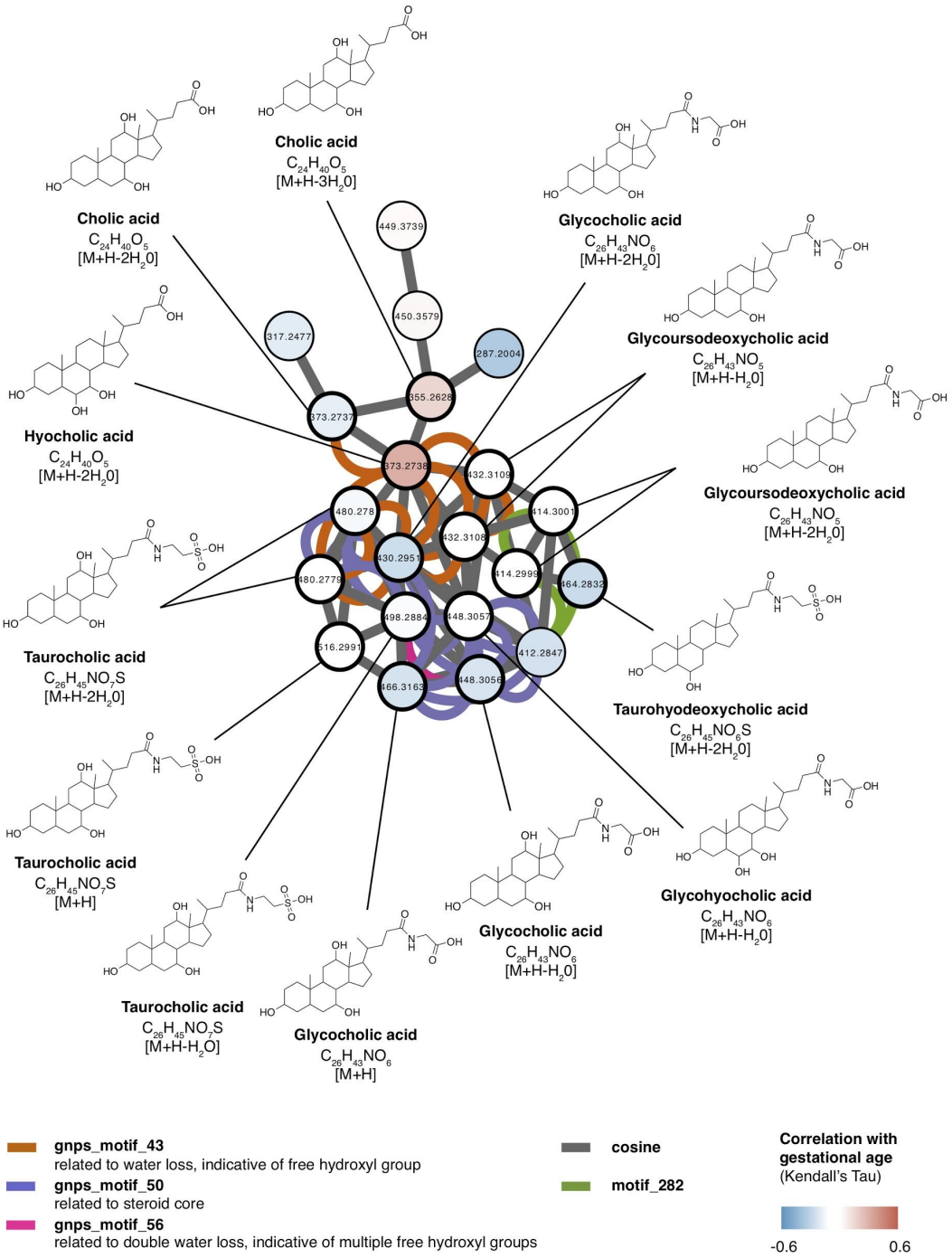

Supplementary Figure 5: Molecular family significantly overrepresented in metabolites correlating with gestational age (P < 0.01) putatively annotated as bile acids using a combination of metabolome mining tools through the MolNetEnhancer workflow. Nodes with bold black borders indicate GNPS spectral library hits with a cosine score > 0.7. For more details on annotated motifs, visit ms2lda.org.

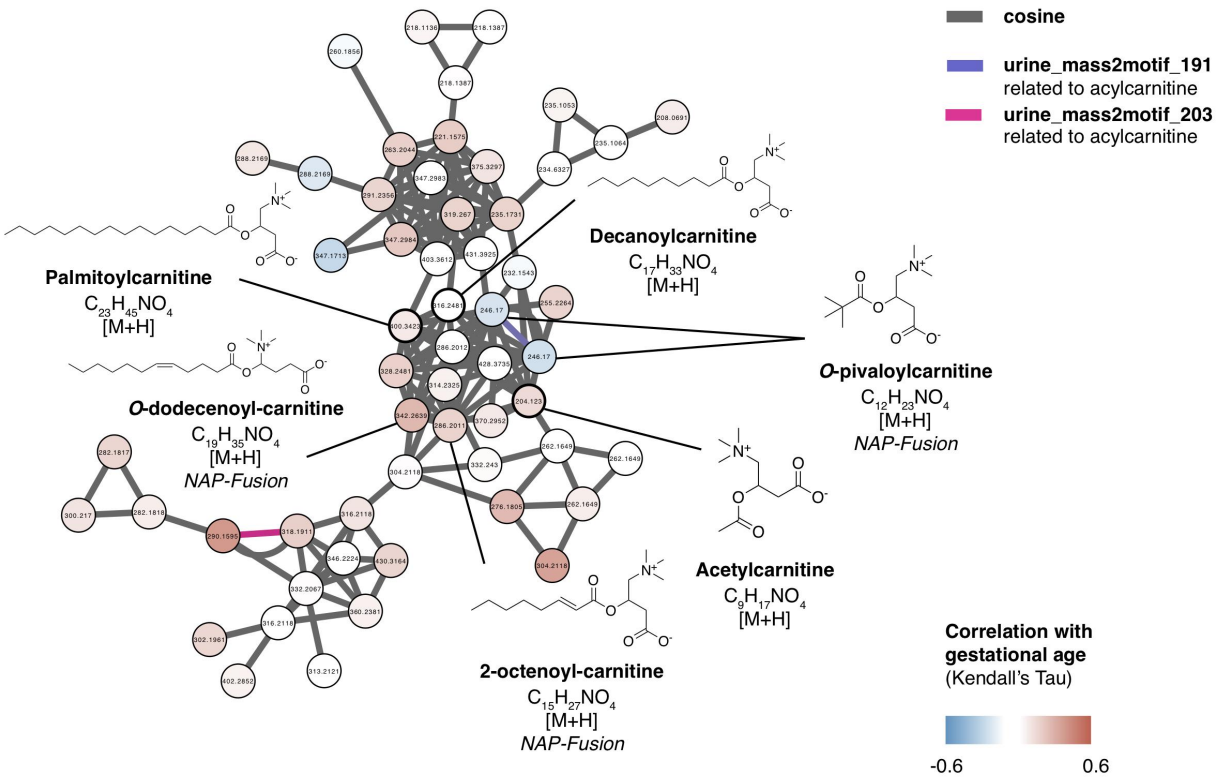

Supplementary Figure 6: Molecular family significantly overrepresented in metabolites correlating with gestational age (P < 0.01) putatively annotated as carnitines using a combination of metabolome mining tools through the MolNetEnhancer workflow. Nodes with bold black borders indicate GNPS spectral library hits with a cosine score > 0.7. For more details on annotated motifs, visit ms2lda.org.

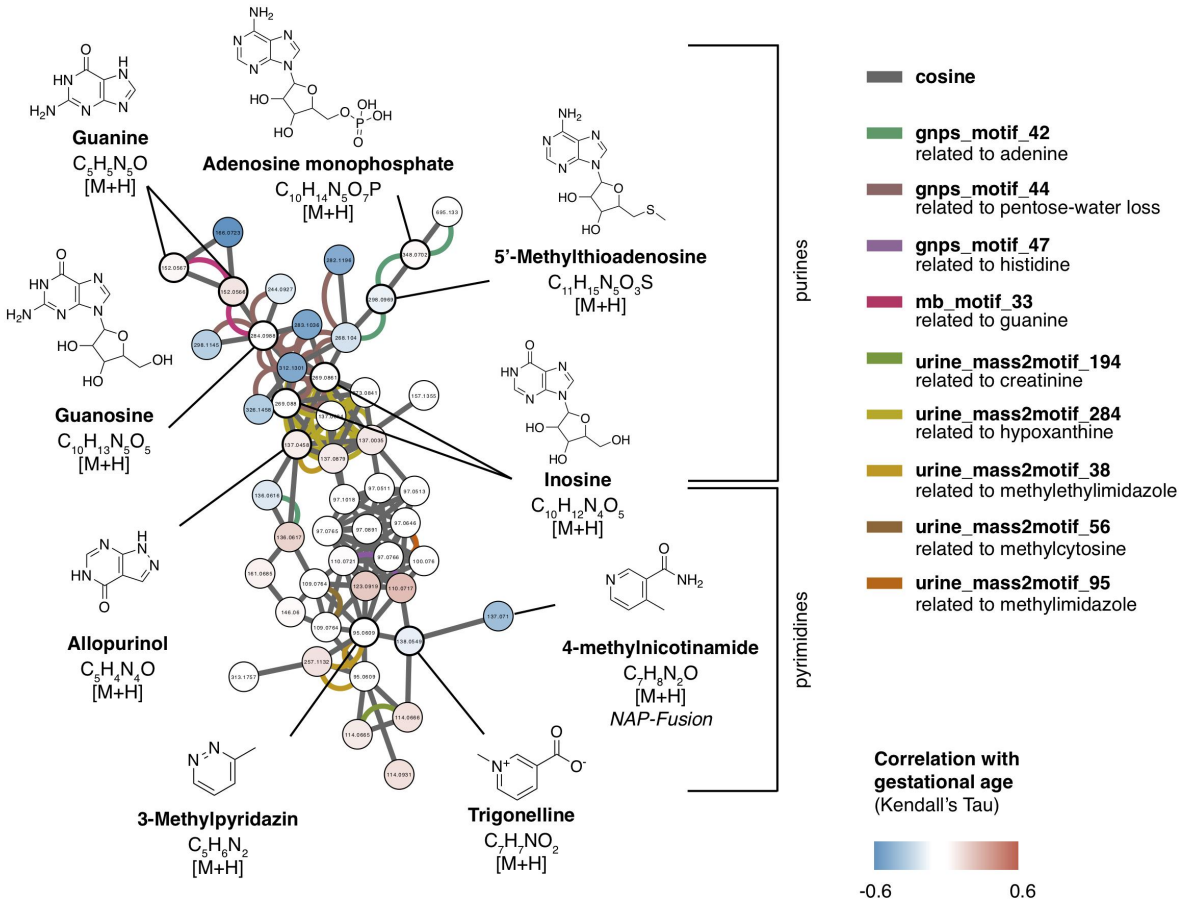

Supplementary Figure 7: Molecular family significantly overrepresented in metabolites correlating with gestational age (P < 0.01) putatively annotated as nucleotides using a combination of metabolome mining tools through the MolNetEnhancer workflow. Nodes with bold black borders indicate GNPS spectral library hits with a cosine score > 0.7. For more details on annotated motifs, visit ms2lda.org.

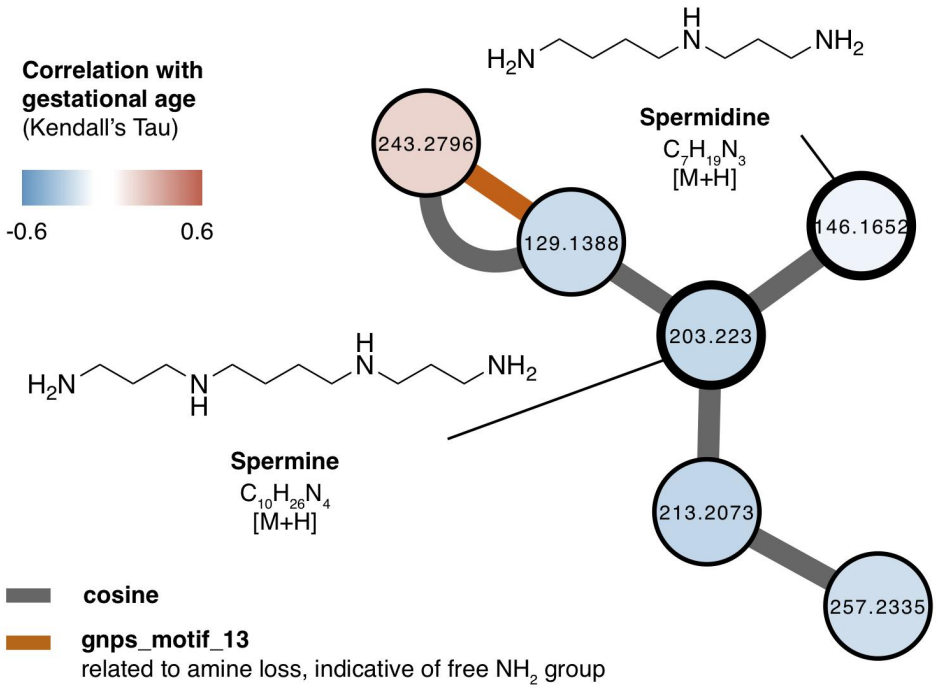

Supplementary Figure 8: Molecular family significantly overrepresented in metabolites correlating with gestational age (P < 0.01) putatively annotated as polyamines using a combination of metabolome mining tools through the MolNetEnhancer workflow. Nodes with bold black borders indicate GNPS spectral library hits with a cosine score > 0.7. For more details on annotated motifs, visit ms2lda.org.

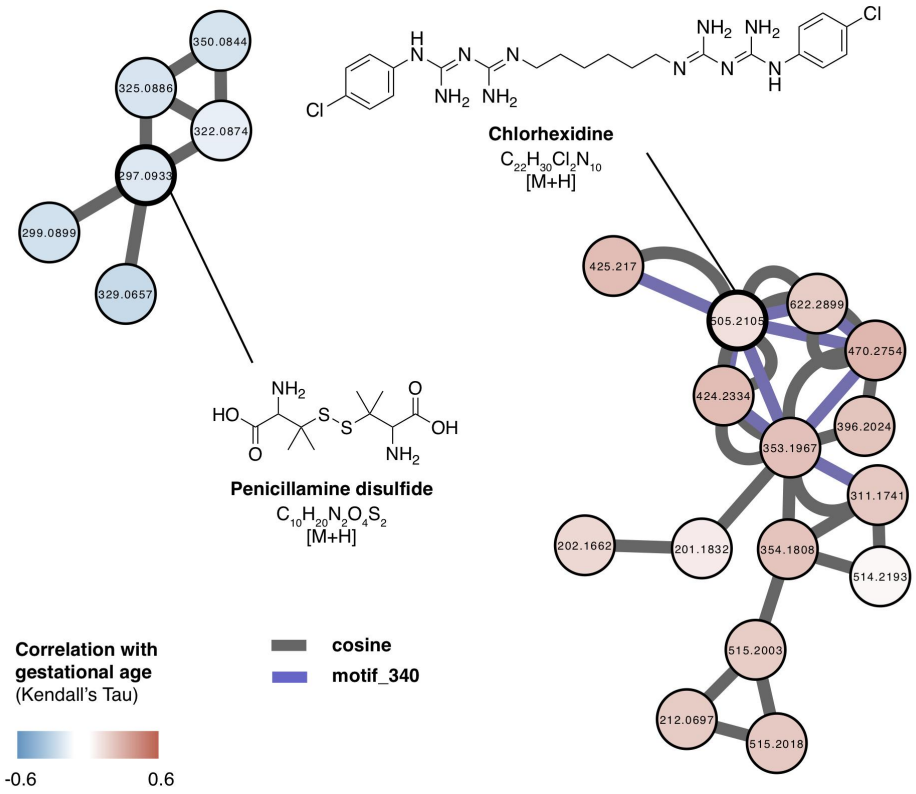

Supplementary Figure 9: Molecular family significantly overrepresented in metabolites correlating with gestational age (P < 0.01) putatively annotated as chlorhexidine and penicillamine disulfide related metabolites using a combination of metabolome mining tools through the MolNetEnhancer workflow. Nodes with bold black borders indicate GNPS spectral library hits with a cosine score > 0.7. For more details on annotated motifs, visit ms2lda.org.

Supplementary Data

Supplementary Data 1: Box plots of forty chemically structurally annotated compounds through GNPS library matching including amino acids, bile acids, nucleotides, peptides, polyamines, antibiotics, sugars and treatment related compounds such as caffeine correlating significantly with gestational age (false-discovery-rate-adjusted $P < 0.05$).

Supplementary Data 2: Spectral mirror plots of forty chemically structurally annotated compounds through GNPS library matching including amino acids, bile acids, nucleotides, peptides, polyamines, antibiotics, sugars and treatment related compounds such as caffeine correlating significantly with gestational age (false-discovery-rate-adjusted $P < 0.05$). Data were extracted automatically using the metabolomics USI tool (http://metabolomics-usi.ucsd.edu/) and mirror plots produced in Python 3.7. using the spectrum_utils package [Wout, 2020].

Supplementary Data 3: Relationship of 100 putatively annotated metabolites with gut maturation, health and microbiome.

Supplementary References

1. Chace DH, De Jesús VR, Lim TH, Hannon WH, Spitzer AR. Tandem mass spectrometric identification of dextrose markers in dried-blood spots from infants receiving total parenteral nutrition. Clin. Chim. Acta 2010; 411: 1806-1816.
2. Groer MW, Luciano AA, Dishaw LJ, et al. Development of the preterm infant gut microbiome: a research priority. Microbiome 2014; 2: 38.
3. Hussain T, Tan B, Ren W, Rahu N, Kalhoro DH, Yin Y. Exploring polyamines: functions in embryo/fetal development. Animal Nutrition 2017; 3, 7-10.
4. Kessner D, Chambers M, Burke R, Agus D, Mallick P. ProteoWizard: open source software for rapid proteomics tools development. Bioinformatics 2008; 24: 2534–2536.
5. Morton JT, Aksenov AA, Nothias LF et al. Learning representations of microbe–metabolite interactions. Nat. Methods 2019; 16: 1306-1314.
6. Myers OD, Sumner SJ, Li S et al. One step forward for reducing false positive and false negative compound identifications from mass spectrometry metabolomics data: new algorithms for constructing extracted ion chromatograms and detecting chromatographic peaks. Anal. Chem. 2017; 89: 8696–8703.
7. Sánchez-Pintos Pérez-Muñuzuri A, Cocho JÁ et al. Evaluation of carnitine deficit in very low birth weight preterm newborns small for their gestational age. J Matern Fetal Neonatal Med. 2016; 29: 933-937.
8. Satouchi M, Watanabe T, Wakabayashi S et al. Digestibility, absorptivity and physiological effects of cellooligosaccharides in human and rat. Journal of Japanese Society of Nutrition and Food Science (Japan) 1998; 49: 143-148.
9. Shannon P, Markiel A, Ozier O et al. Cytoscape: A software environment for integrated models of biomolecular interaction networks. Genome Research 2003; 13: 2498–2504.
10. Sumner LW, Amber A, Barrett D et al. Proposed minimum reporting standards for chemical analysis Chemical Analysis Working Group (CAWG) Metabolomics Standards Initiative (MSI). Metabolomics 2007; 3: 211-221.
11. Timmons J, Chang ET, Wang JY, Rao JN. Polyamines and gut mucosal homeostasis. J Gastrointest Dig Syst. 2012; 20: 2.
12. Tibshirani, R. Regression shrinkage and selection via the lasso. J. R. Stat. Soc. Series B Stat. Methodol. 1996; 73: 9.
13. Ussher JR, Lopaschuk GD, Arduini A. Gut microbiota metabolism of L-carnitine and cardiovascular risk. Atherosclerosis 2013; 231: 456-461.
14. Wout B, spectrum_utils: A Python Package for Mass Spectrometry Data Processing and Visualization. Anal. Chem. 2020; 92: 659-661.
15. Zöhrer E, Resch B, Scharnagl H et al. Serum bile acids in term and preterm neonates. Medicine 2016; 95: 44.